Interface Immobilization Chemistry of *c*RGD-based Peptides Regulates Integrin Mediated Cell Adhesion

Diego Pallarola, Alexander Bochen, Heike Boehm, Florian Rechenmacher, Tariq R. Sobahi, Joachim P. Spatz, and Horst Kessler**

The interaction of specific surface receptors of the integrin family with different extracellular matrix-based ligands is of utmost importance for the cellular adhesion process. A ligand consists of an integrin-binding group, here cyclic RGDfX, a spacer molecule that lifts the integrin-binding group from the surface and a surface anchoring group. *c*(-RGDfX-) peptides are bound to gold nanoparticle structured surfaces via polyproline, polyethylene glycol or aminohexanoic acid containing spacers of different lengths. Although keeping the integrin-binding *c*(-RGDfX-) peptides constant for all compounds, changes of the ligand´s spacer chemistry and length reveal significant differences in cell adhesion activation and focal adhesion formation. Polyproline-based peptides demonstrate improved cell adhesion kinetics and focal adhesion formation compared with common aminohexanoic acid or polyethylene glycol spacers. Binding activity can additionally be improved by applying ligands with two head groups, inducing a multimeric effect. This study gives insights into spacer-based differences in integrin-driven cell adhesion processes and remarkably highlights the polyproline-based spacers as suitable ligand-presenting templates for surface functionalization.

1. Introduction

Cell adhesion is a fundamental process for multicellular organisms, whereas integrins are one of the most important protein families mediating this event.[1] These transmembrane spanning glycoproteins consist of an α- and β-subunit[2] and mediate cell adhesion by connecting the cytoskeleton to proteins of the extracellular matrix (ECM). So far 24 different heterodimeric integrins, which can be classified into four subfamilies, have been identified.[2,3] The members of the RGD recognizing integrin subfamily use the amino acid sequence Arg-Gly-Asp (RGD) as a minimal essential binding motif.[4] Several proteins of the ECM contain this tripeptidic motif, vitronectin (Vn) being one of the most prominent ones.[2a,5] The integrin subtype $\alpha v\beta 3$, which primarily binds to Vn, plays a pivotal role for initial cell adhesion.[6] As cell adhesion is crucial in several physiological processes and important in the development of diseases like thrombosis (blood coagulation), osteoporosis (insufficient bone matrix remodeling), and cancer (angiogenesis and vascularization), this class of proteins has attracted much attention.[2b,7]

Starting from the linear RGD sequence, our group has applied several techniques to restrict the conformational space such as cyclization,[8] incorporation of a d-amino acid[9] and N-methylation,[10] leading to the development of the anti-angiogenic drug *c*(-RGDf(*N*-Me)Val-), also known as Cilengitide.[10a,10d] Cilengitide is currently in clinical phase II for treatment of several cancers. Additionally, targeting of integrins by means of *c*RGD-based compounds has promoted tremendous advances in the biomaterials field and its use for biomedical applications has increased dramatically in the last decade.[7d] Examples for applications include the use of *c*RGD peptides for the development of integrin $\alpha v\beta 3$-targeted radiotracers[11] to image metastatic tumors,[12] as coatings for titanium implants or organic materials to enhance bone healing,[13] and for surface-modification of liposomes for site selective vascular delivery.[14] In all these cases, the successful development of the scaffolds for

Dr. D. Pallarola, Dr. H. Boehm, Prof. J. P. Spatz
Department of New Materials and Biosystems
Max Planck Institute for intelligent Systems
Heisenbergstr. 3, 70569 Stuttgart, Germany
E-mail: spatz@is.mpg.de
Dr. D. Pallarola, Dr. H. Boehm, Prof. J. P. Spatz
Department of Biophysical Chemistry
University of Heidelberg
69120, Heidelberg, Germany
Dr. A. Bochen, Dr. F. Rechenmacher, Prof. H. Kessler
Institute for Advanced Study and Center for Integrated Protein Science
Department Chemie
Technische Universität München
Lichtenbergstr. 4, 85747, Garching, Germany
E-mail: kessler@tum.de

DOI: 10.1002/adfm.201302411

Dr. H. Boehm
CSF Biomaterials and Cellular Biophysics
Max Planck Institute for Intelligent Systems
Heisenbergstr. 3, 70569, Stuttgart, Germany
Prof. T. R. Sobahi, Prof. H. Kessler
Chemistry Department
Faculty of Science
King Abdulaziz University
P.O. Box 80203, Jeddah 21589, Saudi Arabia

integrin adhesion relied on understanding the regulatory interactions between cells and the coating components. Hence, optimization is of utmost importance for many applications.

Synthetic ligands used for integrin attachment to surfaces are modular in structure and contain three typical elements: an integrin-binding head group, a spacer component of variable length and flexibility, and an attachment point for anchorage (e.g., a thiol group for binding to gold). The non *N*-methylated stem peptide *c*(-RGDfV-)[8] constitutes a commonly used head group. Regarding its sequence, it was shown that the 5th position (valine) in this sequence can be substituted by any other amino acid without affecting the activity of the peptide.[15] As a consequence, many studies used head groups consisting of *c*(-RGDfK-), *c*(-RGDfE-), or a corresponding derivative to the side chain of lysine or glutamic acid in conjunction with aliphatic, or polyethylene glycol (PEG)-based spacers.[13a,16] Unfortunately, the introduction of side chain modifications reduced the binding affinity of the ligands to integrins. To retain binding affinity, polyvalent ligands possessing two or more binding motifs were designed.[11c,17] However, those multivalent peptides are bigger in size and the positive effect of multivalency is partially compensated.[17a] A distinctive feature of aliphatic and PEG spacers is their high flexibility. The preferred conformation in PEG is a gauche arrangement and not the fully extended trans.[18] Hence, it is impossible to precisely control their length by means of design and only average length can be estimated. Spacer flexibility may prevent optimal exposure of integrin ligands.

To study cell-ECM adhesion interactions, it is necessary to first reduce the complexity of the research question to a well-defined model system. Diblock-copolymer micelle nanolithography allows the precise positioning of gold nanoparticles (AuNPs) in a quasi hexagonal pattern with a tunable horizontal interparticle distance.[19] Functionalization of the AuNPs with a cyclic adhesive peptide, such as *c*(-RGDfK-), has allowed a number of investigations on integrin-mediated cell adhesion under a wide variety of specific geometrical arrays.[20] In these studies, it was shown that an interparticle distance of less than 70 nm is sufficient to allow for stable cell adhesion, which is characterized by the development of mature focal adhesion (FA) points.[20a]

It is well known that polyproline forms an extended helix of type II (PPII) in aqueous media (see e.g., another study[21] and references cited therein). Within this helix, three proline residues construct a full turn of the helix and the fourth residue (i+3) is precisely above the first. Three prolines elongate the helix by about 9.3 Å. This helical feature of the polyproline sequence has been widely used as ruler for ligand presentation.[22]

Here, we systematically compare the influence of different spacer systems on the binding affinity of a *c*(-RGDfX-)-containing ligand to its primary target, integrin $\alpha v\beta 3$. The ligands were modified with three kinds of spacers: aminohexanoic acid (Ahx), PEG-based spacers, and polyproline sequences, the former two being examples of flexible spacers, the latter an example of a more rigid spacer. In addition, we investigated the effect of dimerization of the polyproline-based spacers (**Figure 1**) on the affinity to integrin $\alpha v\beta 3$. All synthesized peptides were tested in vitro in a competitive ELISA assay using the natural ligand, Vn, and the soluble integrin $\alpha v\beta 3$.[23] These assays showed that *c*RGD bearing polyproline-based spacers displayed significantly higher integrin $\alpha v\beta 3$ binding affinity than those bearing flexible spacers. To address the effect of the

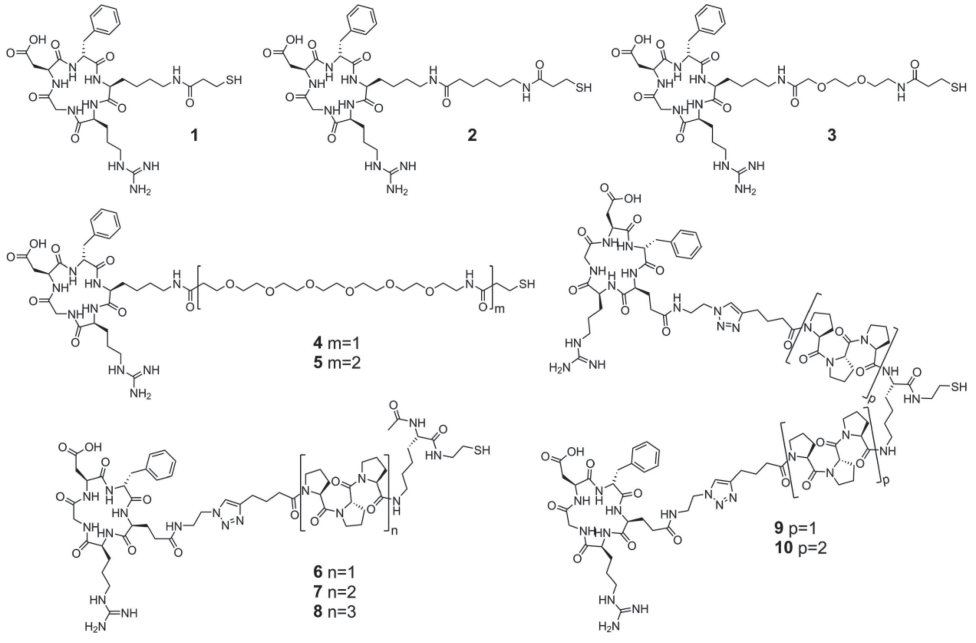

Figure 1. Molecular structure of the peptides studied in this work. **1**–**5**) Ligand peptide comprised of a *c*RGD headgroup, an alkane (**1**–**2**) or PEG (**3**–**5**) type spacer and a thiol anchor for surface attachment. **6**–**10**) Ligand peptide consisting of the *c*RGD headgroup ligated to a polyproline spacer using click chemistry. The lysine linker on the opposite end is acetylated at the Nα position for the attachment of monovalent compounds (**6**–**8**) or used as a branching unit for the synthesis of a peptide head-to-head dimer (**9**–**10**). Spacers linked to each other through the Nα or Nε of the lysine linker possess a thiol anchor for surface attachment (gold-SH bond).

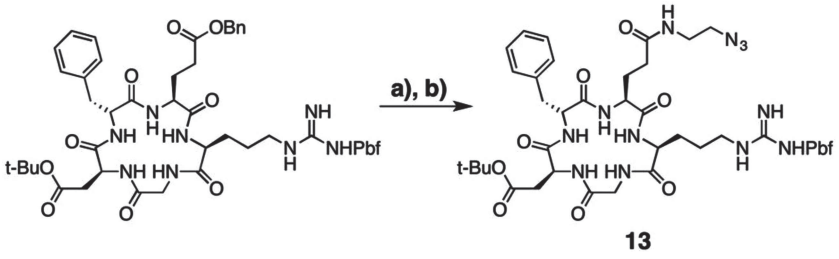

Figure 2. Modification of *c*(-R(Pbf)GD(O^{t}Bu)fE-) (**13**) for application in click chemistry reactions. a) H_2, Pd/C, DMA, 12 h; b) 2-azidoethylamine, HATU, DMF, 1 h.

different spacer systems on cell adhesion behavior, rat embryo fibroblasts (REF52) were plated on surfaces nanostructured with gold nanoparticles of 8 nm diameter with an interparticle distance of 68 nm and functionalized with the respective *c*(-RGDfX-)-spacer derivatives. Immunohistochemical and cell dynamic studies revealed that the nature and length of the ligand-presenting molecule have a profound influence on cell adhesion behavior. Cells attached to substrates functionalized with polyproline-containing peptides exhibited higher spreading rates and FA expression in comparison to those functionalized with analogous aliphatic or PEG-based peptides. We believe that the results presented in this study will reveal useful insights in the field of ligand-oriented drug design and cell-adhesive surfaces.

2. Chemical Synthesis

The required building blocks—the *c*RGD peptide and the spacer unit—were synthesized separately. All peptides were assembled using solid phase synthesis and Fmoc strategy.[24] The linear, side chain-protected sequence of the RGD peptide was synthesized on tritylchloride polystyrene (TCP) resin as support, starting with glycine to prevent racemization during the later cyclization step. The following permanent, orthogonal, side chain protections were used: 2,2,4,6,7-pentamethyldihydrobenzofuran-5-sulfonyl (Pbf) for Arg, *tert*-butyl for Asp, benzyl (Bz) for Glu, and benzyloxycarbonyl (Cbz) for Lys. Amino acids (3.0 equiv.) were coupled stepwise with 2-(1*H*-benzotriazole-1-yl)-1,1,3,3-tetramethyluronium tetrafluoroborate (TBTU, 3.0 equiv.) and *N*-hydroxy-benzotriazole (HOBt, 3.0 equiv.) as coupling reagents and *N,N*-diisopropylamine (DIEA, 6.0 equiv.) as a base. Cleavage from the resin by retention of the side-chain protecting groups occurred using a mixture of DCM/acetic acid/trifluorethanol (7:2:1). Cyclization of the linear peptide was achieved by 2-(7-aza-1*H*-benzotriazole-1-yl)-1,1,3,3-tetramethyluronium hexafluorophosphate (HATU, 2.0 equiv.), HOBT (2.0 equiv.), and DIEA (10 equiv.) using high dilution levels to favor the intramolecular reactions over intermolecular reactions. Finally, hydrogenation of the Bz or Cbz group resulted in the partially protected cyclic peptide. The unprotected glutamic acid of the cyclic peptide was modified by 2-azidoethylamine (4.0 equiv., **11**), HATU (1.05 equiv.), and DIEA (5.0 equiv.) resulting in the azido-modified cyclic peptide **13**, suitable for azide-alkyne 1,3-dipolar cycloaddition (click chemistry) reactions (**Figure 2**).[25] 2-azidoethylamine was synthesized from 2-bromoethylamine hydrochloride (1.0 equiv.) and sodium azide (3.0 equiv.).[26]

Ahx and PEG-based spacer systems were synthesized using the same peptide coupling methodology as described for the synthesis of the linear RGD peptide (see above). The spacer was functionalized by trityl protected 3-mercaptopropionic acid (MPA) as a thiol anchor before being cleaved from the resin by hexafluorisopropanol (HFIP) (20%/DCM). Each spacer (1.0 equiv.) was reacted with *c*(-R(Pbf)GD(O^{t}Bu)fK-) (1.0 equiv.) using HATU (1.0 equiv.) and DIEA (4.0 equiv.). Synthesis of the polyproline-based spacers followed a different Fmoc-based synthesis strategy: The TCP resin was loaded with Fmoc-Lys(Alloc)-OH, Fmoc was removed, the unprotected *Nα* was acetylated by acetic acid anhydride, and the allyloxycarbonyl protecting group (Alloc) was removed by a mixture of *tetrakis*-triphenylphosphin-palladium(0) (0.25 equiv.) and triphenylsilane (10.0 equiv.) in anhydrous DCM. For the synthesis of the polyproline sequence Fmoc-proline-OH (3.0 equiv.), (1-cyano-2-ethoxy-2-oxoethylidenaminooxy) dimethylamino-morpholino-carbenium hexafluorophosphate (COMU,[27] 3.0 equiv.), ethyl(hydroxyimino)cyanoacetate (Oxyma,[28] 3.0 equiv.) and DIEA (6.0 equiv.) were used. The Fmoc group was removed by standard conditions and, as a last step, 5-hexynoic acid (3.0 equiv.) was coupled by COMU (3.0 equiv.) and DIEA (6.0 equiv.) to the polyproline sequence. To obtain divalent peptides the first polyproline sequence was synthesized on the unprotected Lys-*Nα* instead of the acetylation step. The spacer was cleaved from the solid support by HFIP (20%/DCM), ligated to **13** using $CuSO_4$ (1.0 equiv.) and sodium ascorbate (2.0 equiv.) per cyclic peptide in a ^{t}BuOH/H_2O (1:1–2:1) mixture and purified by RP-HPLC.[25,29] The C-terminal carboxylic acid on the lysine was functionalized by 2-(tritylthio)ethylamine **12** (1.0 equiv.), HATU (1.0 equiv.), 1-hydroxy-7-aza-benzotriazole (HOAt, 1.0 equiv.), and DIEA (4.0 equiv.), as a last step. Finally, all remaining protecting groups were removed by trifluoracetic acid/H_2O/triisopropylsilane (95:2.5:2.5) treatment and the peptides were purified by RP-HPLC (**Figure 3**).

3. Results and Discussion

3.1. In Vitro Inhibition of Integrin Binding

A comprehensive list of all the monovalent and divalent *c*RGD ligands and their reference numbers can be found in **Table 1**.

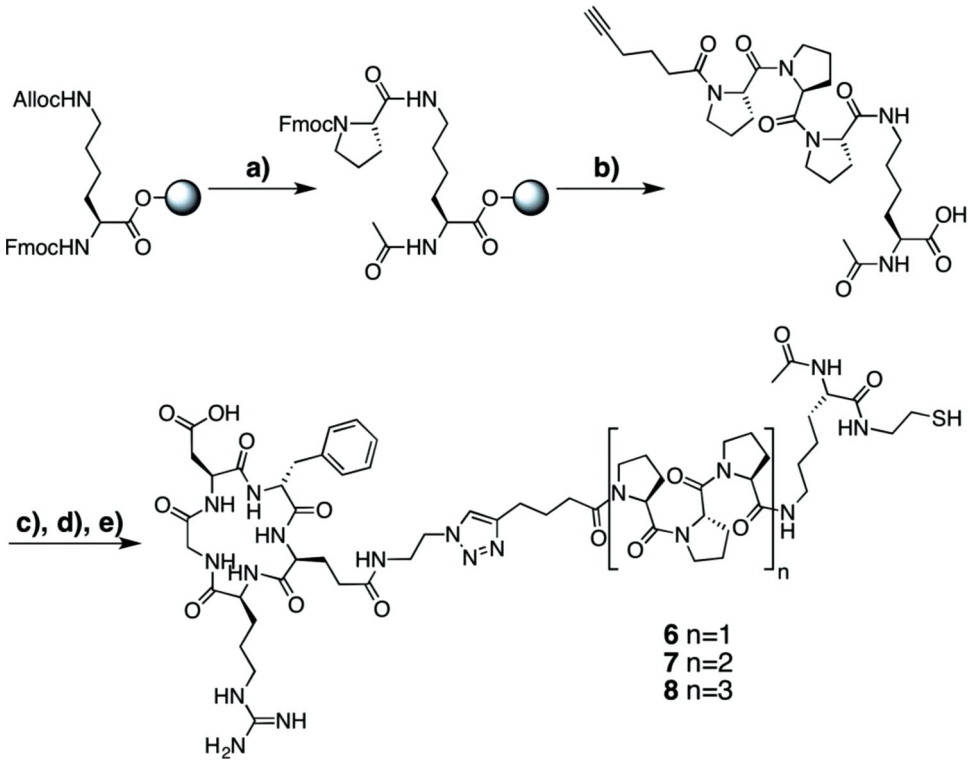

Figure 3. Synthesis of a monomeric proline spacer compound and its ligation with **13**. a) i: 20% piperidine/NMP (Fmoc dpr.); ii: Ac_2O, DIEA, NMP; iii: $Pd(PPh_3)_4$, phenylsilane, anhydrous DCM, 1 h; iv: Fmoc-Pro-OH, COMU, Oxyma, DIEA, NMP, 1 h; (Pro coupling). b) i: repeats of Fmoc dpr (a i) and Pro coupling (a iv), 5-hexynoic acid, COMU, DIEA, NMP, 1h, ii 20% HFIP/DCM; c) **11**, $CuSO_4$, NaAsc., *tert.*-BuOH/H_2O, 70 °C, 3 h; d) Trt-cystamine, HATU, HOAt, DIEA, DMF, 1 h; e) TFA/TIPS/H_2O, 1 h.

Table 1. Inhibition of integrin binding to vitronectin ($\alpha v\beta 3$) by monovalent and divalent *c*RGD pentapeptides using different kinds of spacer systems

Reference number and peptide description	IC_{50}[a] $\alpha v\beta 3$ [nm]
1*c*(-RGDfK-)[MPA]	3.4 (± 0.4)
2*c*(-RGDfK-)[Ahx-MPA]	13.6 (± 2.4)
3*c*(-RGDfK-)[Trigas-MPA]	8.4 (± 2.4)
4*c*(-RGDfK-)[Hegas-MPA]	13.6 (± 3.6)
5*c*(-RGDfK-)[HegasHegas-MPA]	16.5 (± 7.5)
6 Ac-K-[*c*(-RGDfE-)[HexPPP]]-cta	2.4 (± 0.8)
7 Ac-K-[*c*(-RGDfE-)[HexPPPPPP]]-cta	2.5 (± 0.4)
8 Ac-K-[*c*(-RGDfE-)[HexPPPPPPPPP]]-cta	2.1 (± 0.2)
9 [*c*(-RGDfE-)[HexPPP]]$_2$K-cta	0.52 (± 0.04)
10 [*c*(-RGDfE-)[HexPPPPPP]]$_2$K-cta	0.17 (± 0.03)
c(-RGDfK-)[b]	2.6 (± 0.6)
Cilengitide[c]	0.54 (± 0.15)

[a] IC_{50} values were derived from a competitive ELISA using immobilized Vn and soluble integrin $\alpha v\beta 3$;[23a,23b] [b] This cyclic pentapeptide was used as precursor for the design of **1**–**5**;[15] [c] Cilengitide, *c*(-RGDf^{Me}V-)[10d] was used as an internal reference compound for the integrin $\alpha v\beta 3$ ELISA assay. Ahx: 6-amino-hexanoic acid, cta: cystamin, Hegas: heptaethylene glycol amino acid (PEG thiol acid), Hex: 4-(1-(2-aminoethyl)-1*H*-1,2,3-triazol-4-yl)butanoic acid, MPA: mercaptopropionic acid, Trigas: triethylene glycol (PEG).

To evaluate possible differences in the integrin-binding affinity between the ligands containing aliphatic, PEG, monomeric or dimeric polyproline spacers, all synthesized compounds were tested in a competitive ELISA.[23a,23b] Immobilized natural ligand vitronectin (Vn) and soluble integrin $\alpha v\beta 3$ were used. Highly active cyclic pentapeptide Cilengitide, *c*(-RGDf^{Me}V-)[10a,10d] was used as an internal control. The unmodified stem compound *c*(-RGDfK-), which has been described in literature,[15] was included for further comparison.

The integrin $\alpha v\beta 3$ binding affinity of monovalent compounds (**1**–**5**) with aliphatic (**1**: 3.4 nm, **2**: 13.6 nm) or PEG spacers of different length (**3**–**5**: 8.4–16.5 nm) was less than the binding affinity of the unmodified peptide *c*(-RGDfK-) (2.6 nm) (Table 1). For the ligands with aliphatic or PEG spacers the binding affinity additionally decreased with increasing spacer length. Remarkably, this was not the case for monovalent compounds containing polyproline spacers (**6**–**8**). The affinity of the monovalent polyproline containing ligand towards integrin $\alpha v\beta 3$ (2.1–2.5 nm) was comparable to that of unmodified *c*(-RGDfK-) (2.6 nm). Although the shortest polyproline sequence we used consists of only three consecutive proline residues (**6**), the effect of polyproline as the ligand spacer was pronounced. In contrast to aliphatic or PEG spacers, a length-controlled affinity decrease of polyproline containing ligands was not evidenced when increasing the polyproline spacer length to six (**7**) or nine (**8**) proline residues (**Figure 4**).

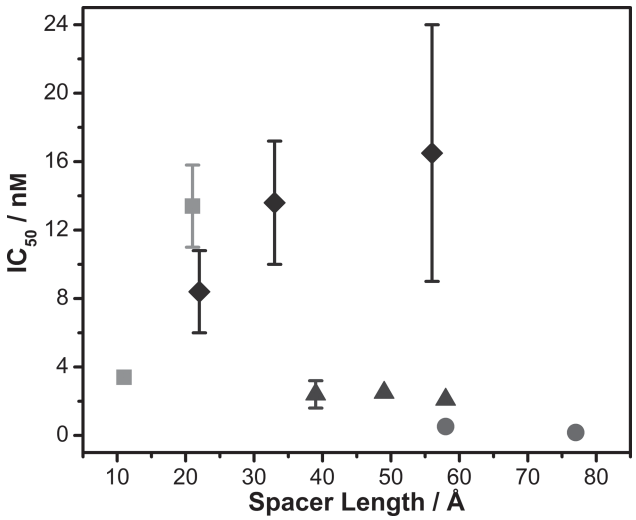

Figure 4. Spacer lengths (Å) and types are correlated to the integrin-binding affinity (IC_{50}). **1–2** (■), **3–5** (◆), **6–8** (▲), **9–10** (●). Spacer length was calculated for the all-*trans* configuration of aliphatic (■) and PEG (◆) spacers, between the Cα Lys(K) and the thiol; Monomeric proline (▲) spacer length was determined between the Cα Glu(E) and the thiol; Dimeric proline (●) spacer length was determined between the Cα Glu(E) via Cα Lys(K) to Cα Glu(E).

The limited binding affinity observed for aliphatic and PEG-based spacer-containing ligands can be ascribed to their high flexibility, which results in coiling and unwanted shielding of the pharmacophoric groups. As these spacer types are seldom found in a fully extended conformation (all-*trans* conformation), the spacer prevents maximum interaction with the integrin-binding site. Obviously, the incorporation of only three consecutive proline residues stiffens the spacer sufficiently to prevent a coiling-related negative effect on the binding affinity of the peptide.

We explored the applicability of the polyproline spacer system for divalent ligands possessing two *c*RGD binding motifs (**9** and **10**). The positive effect of including an extended polyproline sequence inside the ligand on the binding affinity towards integrin $\alpha v\beta 3$ was confirmed for divalent ligands. The extended nature of the polyproline-based dimeric construct displayed, at a fixed distance, an additional epitope able to promote rebinding and therefore increased the relative potency per ligand.[30] Regardless of the spacer length, dimerization gave compounds with sub-nanomolar activities (**9**: 0.52 nm, **10**: 0.17 nm), which is a factor of 4–14 increase to the activities measured for monovalent polyproline peptides (**6–8**: 2.1–2.5 nm). Notably, these affinities were in the range of the binding affinity of Cilengitide *c*(-RGDf^{Me}V-),[10d] the "gold standard" for targeting integrin $\alpha v\beta 3$.

Multivalent compounds first appeared in literature quite some time ago[30,31] and the synthesis of multivalent compounds using Ahx and PEG-based spacers is known.[17a,17b] However, previously described spacers had several disadvantages. In some cases the applied spacers were very short.[17d,32] In another case the addition of tetrameric compounds was necessary to achieve an activity comparable to that of the unmodified cyclic peptide, and a higher activity was obtained only for octamers or even larger compounds.[17f] One report even describes a step-by-step decrease in binding affinity from mono- to di- to tetra-valent compounds.[33] And, one study describes a reduction in the binding affinity with increasing spacer length.[17e]

In this work, we systematically investigated the impact of three different spacer types on the binding affinity of a *c*RGD ligand. We report the direct comparison of Ahx, PEG and polyproline spacers and found superior binding affinity of ligands with spacers containing a polyproline sequence over those with Ahx and PEG spacers.

3.2. Cell Adhesion Experiments

3.2.1. Immunohistochemical Analysis of Cell Spreading and FA Assembly

REF52 cells were plated on *c*RGD-nanopatterns to assess the influence of the different *c*RGD coatings on cell adhesion behavior. Our approach to engineer cellular environments is based on self-organizing spatial positioning of patches of *c*RGD attached to glass via a gold nanopattern. The glass substrates area, which is not covered by gold, is passivated against protein adsorption and cell interactions by a covalently immobilized PEG layer. Such substrates offer the highest possible spatial resolution with respect to the position of *c*RGD patches made of a few single *c*RGD molecules. On such biointerfaces, the regulation of cellular responses is based on a biologically inert background that does not initiate any cell activation, which is then patterned with *c*RGD in well-defined nanoscopic geometries. This approach is very powerful, since it enables the testing of cellular responses to individual *c*RGD nanopatches and their spatial ordering which is very important for comparing the impact of different ligands for integrin activation as reported here. In detail, the glass coverslips were patterned with AuNPs of 8 nm diameter arranged in a quasi-hexagonal structure with an average interparticle distance of 68 nm as reported before.[19] Then, glass area between the AuNPs was passivated with PEG-terminated siloxane.[34] Subsequently, AuNPs were functionalized with a *c*RGD-based thiol ligand as given in Table 1.

In the following, the impact of the three chemically different spacers, the influence of PEG and polyproline spacer length, as well as the effect of divalent polyproline spacer systems on the assembly of FAs and actin fibers were examined. REF52 cells were plated on the individual substrates for 4 h, then fixed and stained for paxillin, nuclei and actin. Every substrate induced cell adhesion and spreading, indicating successful integrin-ligand interactions with all the different compounds (**Figure 5**). However, distinctive differences of adhesion based cell responses are evident between the compounds. In a direct comparison of compounds that differ only with respect to spacer length, an increase in FA density with the spacer length is observed (see Figure S1, Supporting Information). The same observation was made regarding the cell area (see Figure S2, Supporting Information). On all compound-coated surfaces *c*RGD-mediated adhesion induced a dense meshwork of peripheral actin filaments with only a few stress fibers appearing.

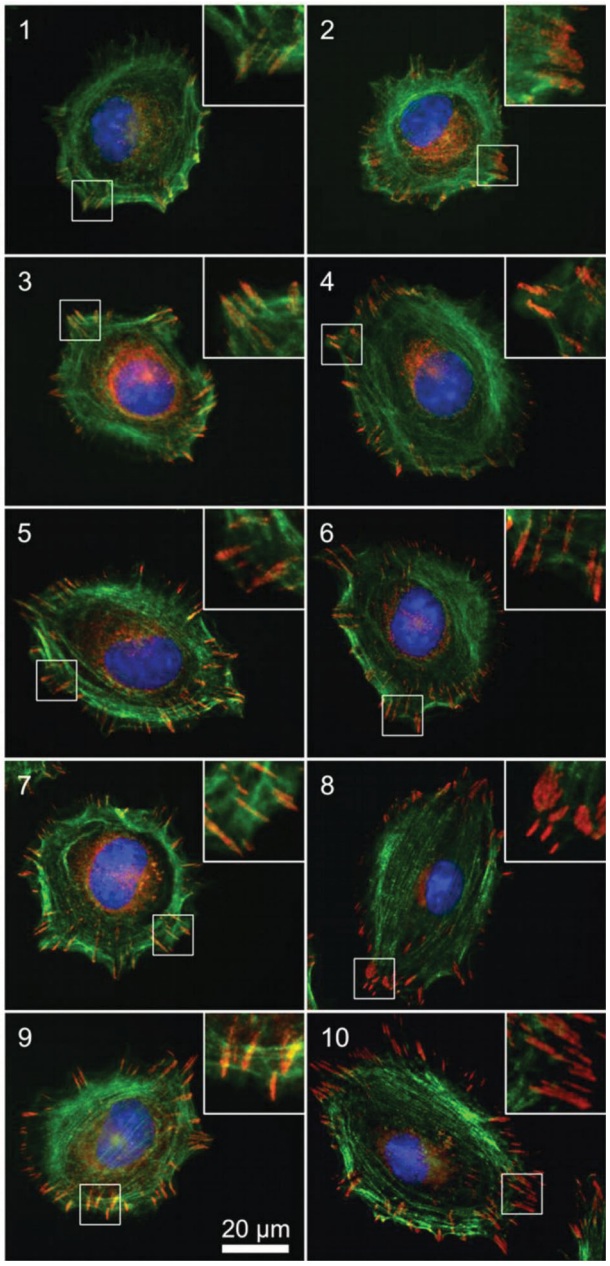

Figure 5. Fluorescent micrographs of representative REF52 cells on nanopatterns functionalized with the different monovalent and divalent *c*RGD peptides (**1**–**10**). Cells were fixed and stained for paxillin (red), nuclei (blue) and actin (green) after an incubation period of 4 h.

There is a seemingly trend that the longer (i.e., compare **3** vs **5**, **6** vs **8**, and **9** vs **10**) and more hydrophilic the spacer is (i.e., compare **2** vs **3**, and **5** vs **8**), the more stress fibers structures were formed inside the cells cytoplasm. Cells did not adhere in control experiments performed on passivated surfaces lacking *c*RGD functionalization. Therefore, cell spreading and FA formation is determined by the presentation of the *c*RGD motif on the nanopatterned surface, which have strong affinity to integrin $\alpha v\beta 3$.[35]

3.2.2. Dynamic Analysis of Cell Adhesion and Spreading

As a next step, we examined the kinetics of cell adhesion and spreading on the differently functionalized substrates. Here, a homemade multiwell array with a PEG passivated and Au-nanostructured glass base plate (**Figure 6**) as in the case of immunohistochemical analysis (Figure 5) was employed. The different wells were functionalized with the different ligands and cell adhesion was monitored in parallel in each of these wells. These studies were conducted with the rat embryo fibroblast cell line REF52, which stably expresses yellow fluorescent protein (YFP)-paxillin,[36] an adhesion associated protein. Therefore, dynamic monitoring of cell adhesion and FA formation could be achieved by fluorescent microscopy utilizing the automated microscopy system Hermes Wiscan.

In **Figure 7**, fluorescence optical microscopy visualization of YFP-paxillin REF52 shows cell spreading and FA maturation over time. Paxillin clusters are shown as bright, mainly elongated spots at the periphery of spreading cells. We have selected and presented in Figure 7 micrographs sequences of cell adhesion corresponding to AuNP-structured surfaces functionalized with compounds **2**, **4**, **6**, and **9**. These sequences adequately illustrate the overall influence of the different kinds of spacers on FA and cell adhesion dynamics.

A quantitative evaluation of the spreading rate was measured by following the projected cell area at different time points up to 540 min (**Figure 8**). Isotropic growth, following a power-law behavior, was observed for all compounds, similar to previous findings.[37] However, striking differences were observed with respect to maximum projected cell area and the time required to reach it. As summarized in **Table 2**, peptides bearing short hydrophobic spacers—compounds **1** and **2**—caused the slowest cellular spreading rate. Both PEG- and polyproline-containing (monovalent and divalent) *c*RGD peptides induced faster cell-spreading rates than those with short hydrophobic spacers. Noteworthy, the cellular spreading rate increased with the spacer length for all compounds. Remarkably, contrary to the surface immobilized cell assays, soluble monovalent compounds with alkanethiol and PEG-thiol spacers (**1**–**5**) showed a reduced affinity to integrin with increasing spacer length in the inhibition assays (Table 1). This reflects the spacer's ability to fold and thereby shield the active moiety, which must be reduced by the interchain van der Waals' interactions in the case of oriented surface immobilization in comparison to the soluble one.[38] It also highlights the role of ligand immobilization for cell adhesion activation. Surfaces functionalized with the hydrophilic polyproline spacers (**6**–**10**) showed faster cell spreading characteristics, which increased with extending spacer length and dimerization. Lag time for spreading initiation was also influenced by the nature and length of the spacers. Cells plated on nanopatterns coated with compounds **6**–**10** (polyproline spacers) and compound **5** (longest PEG-spacer) showed the initiation of cell flattening and spreading between 15 and 18 min after plating. In contrast, compounds **3** and **4** (shorter PEG spacers) and compounds **1** and **2** (short hydrophobic spacers) induced cell flattening around 25 and 40 min after plating, respectively.

3.2.3. Dynamic Analysis of FA Assembly

To further characterize cell adhesion on the nanopatterns coated with the different integrin-binding molecules we studied

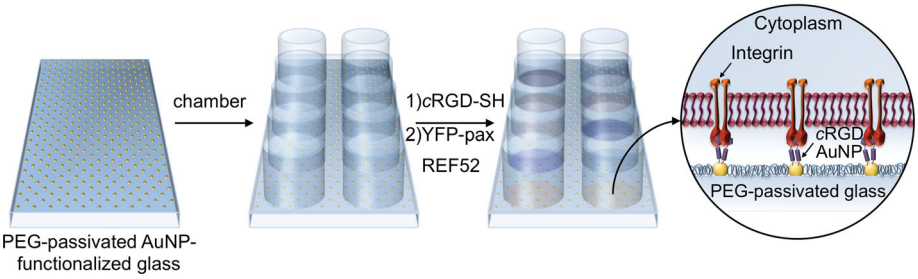

Figure 6. Schematic drawing showing the steps involved in the assembly of the multiwell array employed for cell adhesion dynamics studies. AuNP nanopatterns, as prepared by diblock-copolymer micelle nanolithography on 26 × 76 mm N°1, are glued to a 16-well chamber. 1) Each well is functionalized with a different *c*RGD-based thiol ligand as given in Table 1. 2) YFP-paxillin REF52 cells are plated on each well and visualized with fluorescence microscopy. The magnified area represents the interaction between the integrin extracellular domains and the *c*RGD-coated AuNP.

the dynamics of FA development. No significant differences were revealed in terms of FA size and morphology for the different *c*RGD-coated surfaces. Therefore, measurements of the total area of paxillin patches provided a direct quantification of the density of FAs. **Figure 9** shows the development of the total area of FAs normalized by the projected area of the cell as a function of time. Similar to the observation on spreading initiation, FA development was significantly affected by the type and length of the spacer. As a general rule, functionalization with shorter spacers led to a more delayed development of FAs. This was evidenced by the occurrence of paxillin patches in the cells in Figure 7. Cells on surfaces functionalized with short spacer compounds (**1**–**3**) exhibited well-defined FAs 2.5 h after seeding. On compound **1**, the development of FAs was even slower and only 50% of cells exhibited robust paxillin patches 2.5 h after seeding. In contrast, nanopatterns functionalized with compounds containing longer spacers (**4**–**10**) induced FA development 60–80 min after cells were plated. Compounds **4**–**10** caused similar effects, with one exception. On compound **4**, only 60% of the cells displayed mature FAs 60–80 min after seeding. Differences in the total area of mature FAs after a given amount of time cannot be explained only by a difference in how quickly spreading initiation commences. After subtracting the lag time for spreading initiation from the values in Figure 9, the calculated growth rate of FAs on surfaces functionalized with compounds **4**–**10** was higher than on surfaces functionalized with compounds containing alkane- and short PEG-based spacers. This can be interpreted as an increment of the nucleation rate on substrates with sufficiently exposed ligands (vide infra). The nucleation of FAs can be described as the aggregation of two or more molecules of talin connecting two $\alpha\beta$-integrin dimers through actin filaments.[39] Subsequent recruitment of additional components, for example, paxillin and vinculin, leads to the maturation of these initial clusters into FAs.[40] As the activity of the integrin epitope promotes the formation of stable integrin-*c*RGD complexes, it is also likely that high affinity interactions between receptors and binding sites increase the nucleation frequency. Similar observations

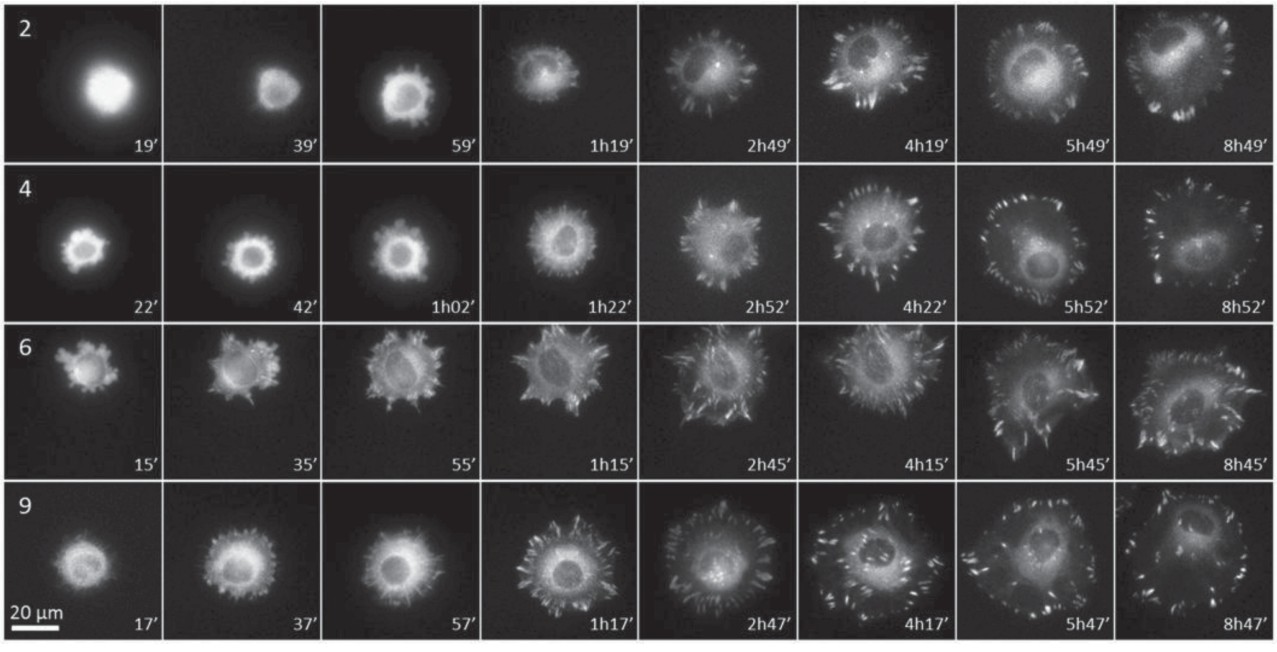

Figure 7. Fluorescence visualization of YFP-paxillin REF52 cell adhesion dynamics on gold nanopatterned surfaces functionalized with compound **2** (*c*(-RGDfK-)[Ahx-MPA]), **4** (*c*(-RGDfK-)[Hegas-MPA]), **6** (Ac-K-[*c*(-RGDfE-)[HexPPP]]-cta), and **9** ([*c*(-RGDfE-)[HexPPP]]$_2$K-cta).

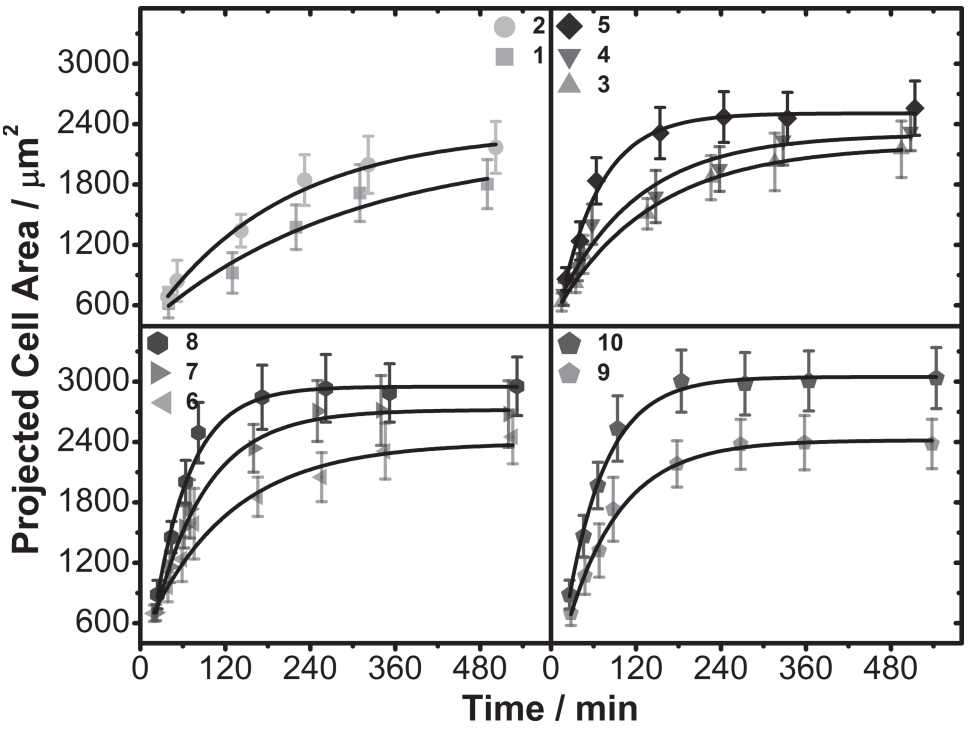

Figure 8. Cell spreading dynamics of YFP-paxillin as observed by Figure 7. Data are presented as mean ± standard deviation. The solid lines in each plot represent the fitting of the time-resolved spreading area data to a one-parameter exp4onential association function.

were reported for 3T3 Swiss fibroblasts plated on thin gold substrates coated with a mixed SAM of *c*RGDfK-terminated alkanethiol and tri(ethylene glycol)-terminated alkanethiol.[35b] There, the authors showed that cells adhering to high-affinity substrates had almost twice as many FAs than cells plated on surfaces with low-affinity coatings.

Interestingly, the shape of the curves obtained for shorter (**1–3**) and longer (**4–10**) spacers (see Figure 9), showed noticeable differences. Whereas on compounds **4–10** cells displayed a sustained increase in the total area of FAs followed by a slow decline towards an asymptotic value, cells plated on surfaces coated with compounds **1–3** exhibited a nearly constant value (meaning that FA area grew by the same proportion as cell area increased). The kinetics of FA assembly is obviously influenced by the quality of ligand presentation. In contrast, the density and distribution of paxillin-based plaques at longer time values (>6 h after seeding) depends on the inherent activity of the pharmacophoric molecule, which in this work remained invariant.

Further analysis of the maximum values of the curves of FA expression dynamics presented in Figure 9 revealed that cells adhering to nanopatterns coated with polyproline-containing compounds induced the highest FA expression (see Figure S3 in the Supporting Information). These results highlight the ability of polyproline-based spacers, more so than alkane and PEG spacers, to efficiently present the active moiety to the cell, thus triggering strong integrin-ligand interactions.

3.2.4. Evaluation of the Ligand Density on AuNP

Activation of integrins triggered by cell-ligand interactions is likely to be affected by the local density of the active ligand, that is, *c*RGD thiol in the present case. Several studies conducted on recognition-driven assembly of proteins showed that the binding affinity of a protein is decreased in high-densely packed assemblies of the target molecule compared to those proteins situated on a surface with lower molecule density.[41] Similarly, Houseman and Mrksich observed that the activity of β-1,4-galactosyltransferase was optimum when the reactant surface molecule (N-acetylglucosamine) constituted 70% of a mixed self-assembled monolayer (SAM).[42] This observation is attributed to steric hindrance between neighboring binding sites when the assembly is highly packed. Therefore, we measured the total amount of chemisorbed thiol species on planar gold substrates by electrochemically reductive desorption in alkaline solution,[43] and calculated the expected number of molecules per particle by assuming an available AuNP surface of 50 nm^2, which accounts to approximately 25% of the total area of a 8 nm-diameter AuNP, while effects of curvature are neglected.[44] The results are summarized in Table 2. The hydrophobic alkane (**1–2**) and more hydrophilic PEG spacers (**3–5**) showed approximately comparative numbers of molecules per gold dot, ranging from 67 to 107. While a longer alkane spacer increased the number of molecules per gold dot from 67 to 98 (**1–2**), the number of molecules per dot was approximately the same for all PEG spacers of different length (**3–5**) and in the range of the longer alkane spacer. Contrary, the number of monomeric polyproline-based peptides (**6–8**) decreased with an increase in the number of proline residues from 54 to 38 molecules per AuNP, respectively. Similar observations were reported in a recent study on oligoproline-based peptides.[45] Due to the hydrophilic nature of the polyproline spacer this is attributed to a reduction in the attractive

Table 2. Influence of the spacer length and the ligand density on the spreading dynamics of YFP-paxillin REF52 cells plated on *c*RGD-functionalized nanopatterns.

Peptide	Spacer length[a)] [Å]	Density[b)] [molecules/50 nm^2]	Time constant[c)] [s]
1	11	67 (± 5)	0.21 (± 0.11)
2	21	98 (± 14)	0.32 (± 0.05)
3	22	92 (± 6)	0.44 (± 0.09)
4	33	107 (± 11)	0.53 (± 0.14)
5	56	96 (± 10)	1.04 (± 0.14)
6	39	54 (± 6)	0.50 (± 0.08)
7	49	44 (± 6)	0.81 (± 0.05)
8	58	38 (± 5)	1.18 (± 0.12)
9	39	18 (± 4)	0.79 (± 0.06)
10	49	15 (± 2)	1.09 (± 0.08)

[a)]Spacer length was calculated for the all-*trans* configuration of aliphatic and PEG spacers between Cα Lys(K) and thiol, and for proline spacers between Cα Glu(E) and thiol; [b)]The surface density of the different thiol-based peptides was estimated by electrochemical reductive desorption conducted on gold planar surfaces. Values are presented as the amount of molecules per 50 nm^2 (50 nm^2 accounts to ~25% of the area of a AuNP with a 8 nm diameter), which is approximately equivalent to the available area on AuNPs attached to PEG-passivated surfaces;[54] [c)]Time constant values were obtained by fitting the spreading data for each peptide functionalized substrate to a one-parameter exponential growth function.

interactions between chains as the spacer length increases. This was also evidenced by a shift in the desorption potential to less negative values (see Figure S4a in the Supporting Information) and is probably caused by a lack of lateral hydrophobic interactions among the polyproline helix, which leads to less compact films. This greatly differs to observations on alkanethiol monolayers on gold, where increasing chain length leads to a denser packing of the monolayer.[38] It can be expected that the extended nature of the polyproline spacers and the reduced coverage density caused by the longer spacer length lead to a greater accessibility of individual *c*RGD moieties by integrins. These results are in full agreement with the observed cell adhesion behavior on nanopatterns functionalized with monovalent polyproline peptides of variable length. Longer spacers caused

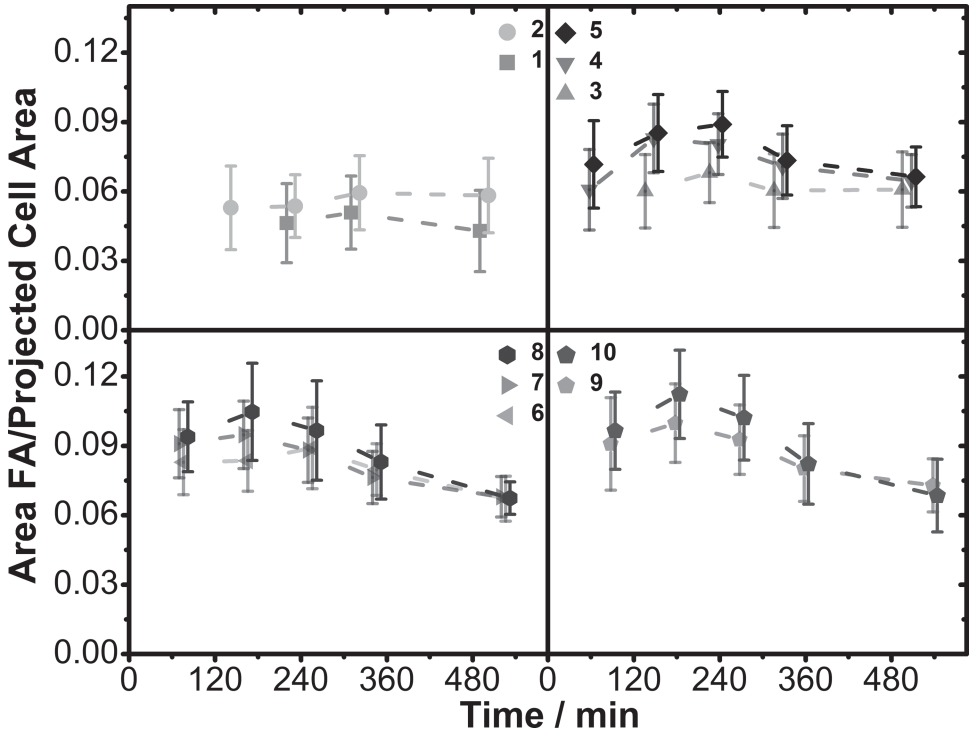

Figure 9. FA expression dynamics followed by fluorescence visualization of YFP-paxillin. Data are presented as mean ± standard deviation. For comparison, FA development is visualized in Figure 7.

a quicker activation of cell adhesion, which can be interpreted as a better accessibility of the ligands by the integrins.[46] QCM measurements performed on mixed SAMs similarly suggest ligand density to be important. These data show that soluble integrin $\alpha v\beta 3$ binding is indeed enhanced when the density of the polyproline-based *c*RGD peptide is diluted with a non-functionalized Pro_3-SH spacer (see Figure S5, Supporting Information).

Similar properties apply for the dimeric polyproline-containing compounds (**9–10**). The packing density of the monolayers decreases with an increasing number of proline residues (see Figure S4b in the Supporting Information). It should be noted that for the same spacer length (calculated between the Cα Glu(E) and the thiol) the coverage density of the dimeric compounds was less than half of that of the monomeric counterparts (i.e., compare **6** vs **9** in Table 2). Therefore, the number of presented *c*RGD moieties is also slightly lower in the case of the dimeric polyproline assembly. This appears reasonable considering that two polyproline helices shared the same anchoring point within the dimers, resulting in even greater space constraints. The higher spreading rates observed for cells plated on nanopatterns coated with polyproline dimers can be ascribed to a better accessibility by integrins due to a less packing density and a more suitable orientation of adjacent *c*RGD molecules towards integrin binding considering the on/off-binding dynamics.

In the case of hydrophobic spacers (**1–2**) the thiolate packing density increased with spacer length due to enhanced attractive interactions between neighboring chains. For compound **2**, density coverage reached values two times larger than the maximum value for compounds of the polyproline series (for details see Supporting Information, Figure S4c). The moderate performance of these monolayers for promoting cell adhesion and spreading can be attributed to the short length and high flexibility of the spacers. Additionally, the close proximity of the bulky *c*RGD molecule and the thiol group is prone to introduce distortions in the organic layer. This effect was stronger for compound **1** than for compound **2**.

PEG-based monolayers displayed a similar trend to that observed for polyproline SAMs. The reductive potential was shifted in a positive direction with increasing PEG chain length (see Figure S4d, Supporting Information), indicating a decrease in the attractive interactions between adjacent chains. Although PEG-based peptides exhibited the highest coverage of all the compounds tested (Table 2), the presence of all PEG chains in a fully extended helical brush configuration, as is commonly observed for SAMs of long chain alkanethiols, is highly unlikely.[47] Under well-solvated conditions PEG chains adopt a highly hydrated coil configuration due to the absence of the necessary driving force to extend their length upon surface immobilization.[48] It is therefore reasonable to expect some degree of coiling of molecular chains on PEG-based SAMs, which ultimately decreases the effective number of spacer molecules that are able to present the *c*RGD binding sequence on a fully extended connector ligand.

3.2.5. Influence of the Spacer Length on Cell Spreading Rate

Integrin binding to the respective ligands depends on integrin activation and is also highly sensitive to the accessibility of the binding motif. Because the induction of conformational changes in the integrin receptors[49] regulate the exposure of the binding site, the ligand-binding domain of the activated integrin heterodimer needs to be located at a defined minimum distance. Due to the relative shortness of the cytoplasmic tails of integrins, the ability to convey conformational changes between the integrin tail and the ligand-binding head group very much depends on the distance between the two.[50] With respect to the data presented in Figure 8, this reports that a successful binding process can only take place if the spacer length can span the distance between the substrate to which it is bound and the integrin-binding domain. To quantitatively assess the impact of the spacer length for each compound series, we plotted the time constant values for each fitted curve against the maximum spacer length (**Figure 10**). Peptides containing hydrophobic (**1–2**) and PEG (**3–5**) spacers were comparable in their cell spreading dynamics (hydrophobic spacers: 0.011 ± 0.016 Å^{-1} s^{-1}; PEG spacers: 0.018 ± 0.007 Å^{-1} s^{-1}). Peptides containing polyproline spacers, in contrast, speeded up cell spreading. Compared to each PEG-containing peptide of equal length, the equivalent polyproline-containing peptides enhanced cell spreading by a factor of about two. Interestingly, monomeric and dimeric polyproline compounds presented similar slope values (monomers **6–8**: 0.036 ± 0.011 Å^{-1} s^{-1}; dimers **9–10**: 0.032 ± 0.014 Å^{-1} s^{-1}), but with higher spreading rates at equal spacer elongation in the case of the dimeric compounds. These results suggest identical contribution of the spacer length to the spreading rate, but improved ligand availability at the nanometric scale, that is, higher integrin-binding affinity, with polyproline dimers.

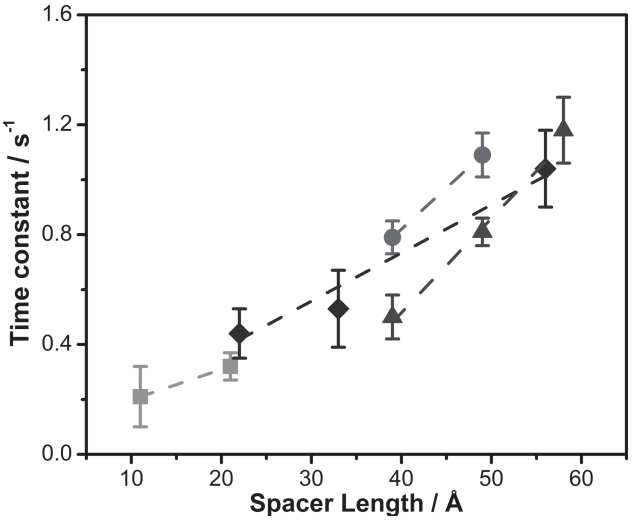

Figure 10. Contribution of spacer length to the spreading rate of YFP-paxillin REF52. Data are presented as mean ± standard deviation. Time constant (k) and spacer length (L) values were extracted from Table 2. Slope values ($\Delta k/\Delta L$) were calculated by a linear fitting for the different spacer series: alkane **1–2** (■): 0.011 ± 0.016 Å^{-1} s^{-1}; polyethylene glycol **3–5** (◆): 0.018 ± 0.007 Å^{-1} s^{-1}; polyproline monomer **6–8** (▲): 0.036 ± 0.011 Å^{-1} s^{-1}; polyproline dimer **9–10** (●): 0.032 ± 0.014 Å^{-1} s^{-1}. The difference between the slope obtained for polyproline spacers (monomer or dimer) and that obtained for polyethylene glycol spacers is significant with 90% level of confidence. No significant (P<0.1) difference was found by comparing the slopes of the alkane and polyethylene glycol series.

4. Conclusion

In this work we have demonstrated the advantages of using a polyproline sequence (rather than an Ahx or a PEG-containing spacer) to connect *c*RGD peptides to artificial substrates used to study integrin-mediated cell adhesion. In two types of different experimental investigations, isolated receptor ELISA assays and cell adhesion studies on AuNP-structured surfaces, the compounds connected by the polyproline spacer resulted in ligands with higher integrin-binding affinity and improved cell adhesion properties than ligands using spacers containing Ahx or PEG. In detail, ELISA assays showed that functionalization of the ligand using an Ahx spacer-containing peptide drastically decreased the ligand binding affinity. Similarly, the application of a PEG spacer of comparable length influenced ligand binding, however at a lesser extent than the alkyl derivative. In addition, increasing the length of the PEG spacer led to less ligand affinity. In contrast, the use of polyproline sequences as *c*RGD-presenting spacer did not alter the ligand binding affinity towards the targeted integrin $\alpha v\beta 3$, independently of its length. Divalent ligands using the polyproline spacer achieved 4 to 14-fold higher ligand binding. The results of ELISA experiments and cell adhesion experiments were comparable for polyproline-based peptides. The quality of cell adhesion is the lowest if a short alkyl chain or Ahx spacer is used and increases with an increasing length of the PEG spacer. More stable cell adhesion is achieved on surfaces coated with monovalent ligand containing a polyproline spacer. Cell adhesion becomes even more mature if the proline spacer is made longer, and even more so when dimeric ligand peptides with polyproline spacers are used. Cell spreading and FA assembly dynamics were highly influenced by the type and length of the spacer. Again, polyproline spacers promoted stronger cell spreading and FA assembly compared to the other spacer types. These results emphasize the advantages of using a polyproline sequence for the backbone of ligand-presenting molecules instead of the commonly applied Ahx and PEG spacers. Compared with alkane- and PEG-based spacers, the more extended characteristic of the polyproline spacers and the low-density assemblies they yield lead to highly accessible *c*RGD moieties, thus enhancing *c*RGD-integrin interactions according to constructive cell spreading and adhesion maturation. These findings may stimulate future development of adhesive surfaces with a higher affinity and could present the possibility to control ligand display more precisely and constructively, thus enabling the study of cell adhesion processes in more defined surroundings.

5. Experimental Section

Chemical Synthesis: All technical solvents were distilled prior to use. Dry solvents were purchased from Sigma-Aldrich or Fluka. Protected Fmoc-amino acids and coupling reagents were purchased from Sigma-Aldrich (Taufkirchen, Germany) Novabiochem (Schwalbach, Germany), Iris Biotech GmbH (Marktredwitz, Germany), PolyPeptide Laboratories (Strasbourg, France), and Medalchemy (Alicante, Spain). TCP-resin was purchased from PepChem (Tübingen, Germany). All other chemicals and organic solvents were purchased from commercial suppliers at the highest purity available and used without further purification. Analytical HPLC was performed using the Amersham Pharmacia Biotech Äkta Basic 10F equipment, with a P-900 pump system, a reversed-phase *YMC*-ODS-A C_{18} column (12 nm pore size, 5 µm particle size, 250 mm × 4.6 mm), and UV detection (UV-900, 220 and 254 nm). The system was run at a flow rate of 1.0 mL/min over 30 min using H_2O (0.1% TFA) and MeCN (0.1% TFA) as solvents. Semi-preparative HPLC was performed using a Waters Breeze System, including a 1525 Pump, a UV-Detector 2487 Dual (220 and 254 nm), and the Driver Software Breeze vers. 3.20. As column material we used: *YMC*-ODS-A C_{18} (12 nm pore size, 5 µm particle size, 250 mm × 20 mm), *YMC*-ODS-AQ C_{18} (12 nm pore size, 5 µm particle size, 250 mm × 20 mm) or *YMC*basic (proprietary pore size, 5 µm particle size, 250 mm × 20 mm). HPLC-ESI-MS analyses were performed on a Hewlett Packard Series HP 1100 with a Finnigan LCQ mass spectrometer using a *YMC*-Hydrosphere C_{18} column (12 nm pore size, 3 µm particle size, 125 mm × 2.1 mm) or a *YMC*-Octyl C_8 column (20 nm pore size, 5 µm particle size, 250 mm × 2.1 mm). The system uses H_2O (0.1% formic acid) and MeCN (0.1% formic acid) as eluents. Standard peptide coupling techniques were employed. Yields were not optimized. All tested compounds exhibited ≥ 95% purity, as determined by RP-HPLC-(MS). Peptide synthesis was carried out using TCP resin following standard Fmoc-strategy.[24] A detailed description of the synthetic procedures is presented in the Supplementary Information section.

Integrin Binding Assay (Vn/αvβ3): The inhibiting activity of the integrin ligands was determined in a solid-phase binding assay using coated extracellular matrix protein and soluble integrin. Binding of the integrin was detected by a specific antibody in an enzyme-linked immune sorbent assay (ELISA). The assay was based on a previously reported method with several modifications.[51] Flat-bottom 96-well ELISA plates (*BRAND*, Wertheim, Germany) were coated overnight at 4 °C with 100 µL/well of 1.0 µg/mL vitronectin (Millipore, Schwalbach/Ts., Germany) in carbonate-buffer (15 mm Na_2CO_3, 35 mm $NaHCO_3$, pH 9.6). Each well was then washed with PBST buffer (137 mm NaCl, 2.7 mm KCl, 10 mm Na_2HPO_4, 2 mm KH_2PO_4, 0.01% Tween 20, pH 7.4, 3 × 200 µL) and blocked for 1 h at room temperature with 150 µL/well of TSB-buffer (20 mm Tris-HCl, 150 mm NaCl, 1 mm $CaCl_2$, 1 mm $MgCl_2$, 1 mm $MnCl_2$, pH 7.5, 1% BSA). After being washed three times with PBST, equal volumes of internal standard (Cilengitide) or test compounds were mixed with 2.0 µg/mL human integrin $\alpha v\beta 3$ (Millipore, Schwalbach/Ts., Germany). The final dilution in TSB buffer was 1.0 µg/mL for integrin $\alpha v\beta 3$ and ranged between 0.00013 and 10 µm for the inhibitors. The solutions (100 µL/well) were incubated for 1 h at room temperature. The plate was washed three times with PBST buffer and 100 µL/well of 2.0 µg/mL primary antibody mouse anti-human CD51/61 (BD Biosciences, Heidelberg, Germany) was added to the plate. After incubation for 1 h at room temperature, the plate was washed three times with PBST. 100 µL/well of 1.0 µg/mL of secondary peroxidase-labeled antibody (anti-mouse IgG-POD, Sigma-Aldrich, Taufkirchen, Germany) was added to the plate and incubated for 1 h at room temperature. After washing the plate three times with PBST, 50 µL/well of SeramunBlau fast (*Seramun Diagnostic GmbH,* Heidesee, Germany) was added and incubated for 5 min at room temperature. The reaction was stopped with 50 µL/well of 3 m H_2SO_4 and absorbance was measured at 450 nm with a plate reader (POLARstar Galaxy, BMG Labtechnologies). Each compound concentration was tested in duplicate and the resulting inhibition curves were analyzed using OriginPro 7.5G software. In these measurements, the inflection point represents the IC_{50} value. Each plate contained Cilengitide as internal standard.

Biofunctionalized Nanopatterns: AuNP quasi-hexagonal patterns were prepared on glass coverslips by means of diblock-copolymer micelle nanolithography as previously described.[19] Briefly, substrates were dip-coated with a solution of polystyrene(1056)-block-poly[2-vinylpyridine($HAuCl_4$)0.25](495) (Polymer Source Inc., Canada) diblock copolymer micelles in *o*-xylene at a constant pulling rate of 1 mm/s and subsequently subjected to H_2:Ar 1:10 plasma treatment (350 W, 0.4 mbar, 90 min). Then, substrates were treated thermally in an oven at 500 °C for 48 h. This procedure provided nanopatterns consisting of 8 nm high AuNPs (as measured by atomic force microscopy) with an interparticle distance between adjacent AuNPs of 68 ± 9 nm

(determined by scanning electron microscopy). Subsequently, the area between Au nanoparticles was passivated with mPEG-triethoxysilane (2000) to prevent non-specific adhesion according to a procedure described elsewhere.[34] For immunohistochemical experiments, gold nanopatterns on 20 × 20 mm N°1 glass coverslips (Carl Roth, Germany) were employed, whereas cell dynamics experiments were performed on 26 × 76 mm N°1 glass coverslips (Thermo Scientific, Germany). In the latter case, a 16-well Lab-Tek chamber was glued onto the nanopatterned surface with a biocompatible adhesive, named Twinsil (Picodent, Germany). This configuration allowed high throughput screening of the entire set of *c*(-RGDfX-)-based molecules using a single surface. Each well, in the case of the multiple-well array, or each 20 mm × 20 mm surface was functionalized with the corresponding integrin-binding molecule at a concentration of 25 µm in MilliQ water for 2 h at room temperature. Physisorbed material was removed by exhaustive rinsing with MilliQ water and PBS. Cell experiments were carried out immediately after this step.

Cell Culture: REF52 (rat embryo fibroblast) wild type (WT) cells and REF52 cells expressing yellow fluorescent protein (YFP)-paxillin fusion proteins[36] were a kind gift of Benjamin Geiger (Weizmann Institute of Science, Rehovot, Israel). REF52 WT cells and YFP-paxillin REF52 cells were cultured in DMEM medium supplemented with 10% FBS and 1% L-glutamin (Invitrogen, Germany) at 37 °C and 5% CO_2. For adhesion experiments, cells in culture were rinsed with PBS at 37 °C and adherent cells removed from the culture surface by treatment with trypsin-EDTA 0.25% for 5 min at 37 °C. Cells were plated at a density of 150 cells/mm^2 on the functionalized surfaces in DMEM containing 1% FBS, 1% L-glutamin and 100 units/mL penicillin-streptomycin (Invitrogen, Germany), followed by incubation at 37 °C and 5% CO_2.

Immunofluorescence Staining: After 4 h on the nanopatterned surfaces, REF52 WT cells were washed with PBS at 37 °C and fixed with 2.5% paraformaldehyde in PBS for 10 min. Cells were then permeabilized with 0.1% Triton X-100 in PBS, blocked with 5% goat serum (Invitrogen, Germany) in PBS for 1 h at room temperature, and incubated with a 1:100 dilution of rabbit anti-paxillin (Abcam, USA) for 1 h at room temperature. Then, cells were labeled with a 1:100 dilution of anti-rabbit Alexa 594-conjugated secondary antibody (Invitrogen, Germany) in 5% goat serum in PBS for 1 h at room temperature. Filamentous actin and nuclei were labeled with Alexa 488-conjugated phalloidin and DAPI (Invitrogen, Germany), respectively. Cells were examined with a 63/1.25 Oil Ph3 Antiflex Plan-Neofluar objective (Carl Zeiss, Germany) using an Axiovert 200 fluorescent microscope (Carl Zeiss, Germany) equipped with a Hamamatsu digital CCD camera (model C10600–10B-H; Hamamatsu Photonics, Germany). Image processing was done using the Axiovision Image viewer (Carl Zeiss, Germany).

Cell Dynamics Experiments: YFP-paxillin expressing REF52 cells were plated on the multiple-well array and immediately mounted on the thermostatized stage of the microscope at 37 °C under 5% CO_2 and controlled humidity. Immunofluorescence visualization of cells was performed with a Hermes WiScan (Idea Bio-Medical, Israel) system equipped with an Andor digital CCD camera (model iXon 897; Andor Technology, USA), a fast AutoFocus device[52] and an automated stage. Cells were examined with a U Plan FL N 60×/0.9 objective (Olympus, Japan) at different time intervals starting 10 min after plating. Sets of 76 images per well were taken, with an average acquisition time of 0.6 s per image. Image processing and analysis were performed using the image analysis platform WiSoft (Idea Bio-Medical, Israel). Briefly, images were first subjected to a low-pass filtration to smooth out non-uniformities in intensity. After that, images were subjected to a high-pass filtration to flatten the image and enhance edges. Finally, the resulting processed images were used for optimizing parameters (threshold, maximum and minimum size of the patches, etc.) for the segmentation module, which defines objects based on their intensity and morphological attributes. Each time point of the corresponding *c*(-RGDfX-)-based compound was based on the evaluation of 50 cells from at least two different multiple-well arrays.

Electrochemical Experiments: SAMs of the different thiol-based *c*RGD peptides were prepared on flamed annealed gold substrates (Arrandees, Germany) and were subjected to reductive electrodesorption of thiols. The charge density of the cathodic peaks was taken as an indication of the surface coverage by the different *c*RGD-thiol derivatives.[53] For a detailed description, please refer to the Supporting Information.

Supporting Information

Supporting Information is available from the Wiley Online Library or from the author.

Acknowledgements

D.P. and A.B. contributed equally to this work. The authors gratefully acknowledge financial support from the International Graduate School of Science and Engineering (IGSSE), from the TUM Graduate School (TUM GS) and the Max Planck Society. Part of the research leading to these results received funding from the European Union Seventh Framework Programme (FP7/2007–2013) under grant agreement n° NMP4-LA-2009–229289 NanoII and n° NMP3-SL-2009–229294 NanoCARD. We gratefully thank for the technical and financial support from King Abdulaziz University KAU (grant No. HiCi/25–3–1432). The group is part of the excellence cluster CellNetworks at the University of Heidelberg. J.P.S. is the Weston Visiting Professor at the Weizmann Institute of Science.

Received: July 17, 2013
Revised: August 28, 2013
Published online: October 16, 2013

[1] B. Geiger, J. P. Spatz, A. D. Bershadsky, *Nat. Rev. Mol. Cell Biol.* **2009**, *10*, 21.
[2] a) R. O. Hynes, *Cell* **1992**, *69*, 11; b) B. H. Luo, C. V. Carman, T. A. Springer, *Annu. Rev. Immunol.* **2007**, *25*, 619.
[3] M. Barczyk, S. Carracedo, D. Gullberg, *Cell Tissue Res.* **2010**, *339*, 269.
[4] a) E. Ruoslahti, M. Pierschbacher, *Science* **1987**, *238*, 491; b) E. Ruoslahti, *Annu. Rev. Cell Dev. Biol.* **1996**, *12*, 697; c) J. D. Humphries, A. Byron, M. J. Humphries, *J. Cell Sci.* **2006**, *119*, 3901.
[5] a) E. Zamir, B. Geiger, *J. Cell Sci.* **2001**, *114*, 3577; b) R. O. Hynes, *Science* **2009**, *326*, 1216.
[6] a) S. P. Massia, J. A. Hubbell, *J. Cell Biol.* **1991**, *114*, 1089; b) K. Hodivala-Dilke, *Curr. Opin. Cell Biol.* **2008**, *20*, 514.
[7] a) A. Meyer, J. Auernheimer, A. Modlinger, H. Kessler, *Curr. Pharmaceut. Design* **2006**, *12*, 2723; b) Z. F. Liu, F. Wang, X. Y. Chen, *Drug Dev. Res.* **2008**, *69*, 329; c) D. Cox, M. Brennan, N. Moran, *Nat. Rev. Drug Discovery* **2010**, *9*, 804; d) S. L. Goodman, M. Picard, *Trends Pharmacol. Sci.* **2012**, *33*, 405.
[8] M. Aumailley, M. Gurrath, G. Müller, J. Calvete, R. Timpl, H. Kessler, *FEBS Lett.* **1991**, *291*, 50.
[9] R. Haubner, D. Finsinger, H. Kessler, *Angew. Chem. Int. Edit.* **1997**, *36*, 1375.
[10] a) M. A. Dechantsreiter, E. Planker, B. Mathä, E. Lohof, G. Hölzemann, A. Jonczyk, S. L. Goodman, H. Kessler, *J. Med. Chem.* **1999**, *42*, 3033; b) J. Chatterjee, C. Gilon, A. Hoffman, H. Kessler, *Acc. Chem. Res.* **2008**, *41*, 1331; c) J. Chatterjee, F. Rechenmacher, H. Kessler, *Angew. Chem. Int. Ed.* **2013**, *52*, 254; d) C. Mas-Moruno, F. Rechenmacher, H. Kessler, *Anticancer Agents Med. Chem.* **2010**, *10*, 753.
[11] a) G. B. Sivolapenko, D. Skarlos, D. Pectasides, E. Stathopoulou, A. Milonakis, G. Sirmalis, A. Stuttle, N. S. Courtenay-Luck,

K. Konstantinides, A. A. Epenetos, *Eur. J. Nucl. Med.* **1998**, *25*, 1383; b) W. B. Cai, D. W. Shin, K. Chen, O. Gheysens, Q. Z. Cao, S. X. Wang, S. S. Gambhir, X. Y. Chen, *Nano Lett.* **2006**, *6*, 669; c) M. Schottelius, B. Laufer, H. Kessler, H.-J. Wester, *Acc. Chem. Res.* **2009**, *42*, 969; d) S. Maschauer, J. Einsiedel, R. Haubner, C. Hocke, M. Ocker, H. Huebner, T. Kuwert, P. Gmeiner, O. Prante, *Angew. Chem. Int. Ed.* **2010**, *49*, 976; e) R. Haubner, A. J. Beer, H. Wang, X. Chen, *Eur. J. Nucl. Med. Mol. Imaging* **2010**, *37*, S86; f) Y. Zhou, S. Chakraborty, S. Liu, *Theranostics* **2011**, *1*, 58; g) J. Notni, K. Pohle, H.-J. Wester, *Nucl. Med. Biol.* **2013**, *40*, 33.

[12] a) R. Haubner, W. A. Weber, A. J. Beer, E. Vabuliene, D. Reim, M. Sarbia, K. F. Becker, M. Goebel, R. Hein, H. J. Wester, H. Kessler, M. Schwaiger, *PLoS Med.* **2005**, *2*, 244; b) A. J. Beer, M. Schwaiger, in *Molecular Imaging: Methods and Protocols*, Vol. *680* (Ed: K. Shah), **2011**, 183.

[13] a)M. Kantlehner, D. Finsinger, J. Meyer, P. Schaffner, A. Jonczyk, B. Diefenbach, B. Nies, H. Kessler, *Angew. Chem. Int. Ed.* **1999**, *38*, 560; b) B. Jeschke, J. Meyer, A. Jonczyk, H. Kessler, P. Adamietz, N. M. Meenen, M. Kantlehner, C. Goepfert, B. Nies, *Biomaterials* **2002**, *23*, 3455; c) U. Hersel, C. Dahmen, H. Kessler, *Biomaterials* **2003**, *24*, 4385; d) S. Rammelt, T. Illert, S. Bierbaum, D. Scharnweber, H. Zwipp, W. Schneiders, *Biomaterials* **2006**, *27*, 5561.

[14] R. Srinivasan, R. E. Marchant, A. Sen Gupta, *J. Biomed. Mater. Res. A* **2010**, *93A*, 1004.

[15] R. Haubner, R. Gratias, B. Diefenbach, S. L. Goodman, A. Jonczyk, H. Kessler, *J. Am. Chem. Soc.* **1996**, *118*, 7461.

[16] a) J. Auernheimer, D. Zukowski, C. Dahmen, M. Kantlehner, A. Enderle, S. L. Goodman, H. Kessler, *ChemBioChem* **2005**, *6*, 2034; b) E. Lieb, M. Hacker, J. Tessmar, L. A. Kunz-Schughart, J. Fiedler, C. Dahmen, U. Hersel, H. Kessler, M. B. Schulz, A. Göpferich, *Biomaterials* **2005**, *26*, 2333; c) S. Kalinina, H. Gliemann, M. Lopez-Garcia, A. Petershans, J. Auernheimer, T. Schimmel, M. Bruns, A. Schambony, H. Kessler, D. Wedlich, *Biomaterials* **2008**, *29*, 3004; d) K. A. Kilian, M. Mrksich, *Angew. Chem. Int. Ed.* **2012**, *51*, 4891.

[17] a) G. Thumshirn, U. Hersel, S. L. Goodman, H. Kessler, *Chem.-Eur. J.* **2003**, *9*, 2717; b) D. Lössner, H. Kessler, G. Thumshirn, C. Dahmen, B. Wiltschi, M. Tanaka, W. Knoll, E. K. Sinner, U. Reuning, *Anal. Chem.* **2006**, *78*, 4524; c) L. L. Kiessling, J. E. Gestwicki, L. E. Strong, *Angew. Chem. Int. Ed.* **2006**, *45*, 2348; d) Z. B. Li, W. B. Cai, Q. Z. Cao, K. Chen, Z. H. Wu, L. N. He, X. Y. Chen, *J. Nucl. Med.* **2007**, *48*, 1162; e) H. Kubas, M. Schafer, U. Bauder-Wust, M. Eder, D. Oltmanns, U. Haberkorn, W. Mier, M. Eisenhut, *Nucl. Med. Biol.* **2010**, *37*, 885; f) C. Wangler, S. Maschauer, O. Prante, M. Schafer, R. Schirrmacher, P. Bartenstein, M. Eisenhut, B. Wangler, *Chembiochem* **2010**, *11*, 2168.

[18] M. L. Alessi, A. I. Norman, S. E. Knowlton, D. L. Ho, S. C. Greer, *Macromolecules* **2005**, *38*, 9333.

[19] R. Glass, M. Möller, J. P. Spatz, *Nanotechnology* **2003**, *14*, 1153.

[20] a) M. Arnold, E. A. Cavalcanti-Adam, R. Glass, J. Blümmel, W. Eck, M. Kantlehner, H. Kessler, J. P. Spatz, *ChemPhysChem* **2004**, *5*, 383; b) M. Arnold, V. C. Hirschfeld-Warneken, T. Lohmüller, P. Heil, J. Blummel, E. A. Cavalcanti-Adam, M. López-García, P. Walther, H. Kessler, B. Geiger, J. P. Spatz, *Nano Lett.* **2008**, *8*, 2063; c) M. Arnold, M. Schwieder, J. Blümmel, E. A. Cavalcanti-Adam, M. López-García, H. Kessler, B. Geiger, J. P. Spatz, *Soft Matter* **2009**, *5*, 72; d) J. H. Huang, S. V. Grater, F. Corbellinl, S. Rinck, E. Bock, R. Kemkemer, H. Kessler, J. D. Ding, J. P. Spatz, *Nano Lett.* **2009**, *9*, 1111; e) I. Platzman, C. A. Muth, C. Lee-Thedieck, D. Pallarola, R. Atanasova, I. Louban, E. Altrock, J. P. Spatz, *RSC Adv.* **2013**, *3*, 13293.

[21] M. Moradi, V. Babin, C. Roland, T. A. Darden, C. Sagui, *Proc. Natl. Acad. Sci. U. S. A.* **2009**, *106*, 20746.

[22] a) L. Crespo, G. Sanclimens, B. Montaner, R. Pérez-Tomás, M. Royo, M. Pons, F. Albericio, E. Giralt, *J. Am. Chem. Soc.* **2002**, *124*, 8876; b) Y. A. Fillon, J. P. Anderson, J. Chmielewski, *J. Am. Chem. Soc.* **2005**, *127*, 11798; c) G. Sanclimens, L. Crespo, E. Giralt, F. Albericio, M. Royo, *J. Org. Chem.* **2005**, *70*, 6274; d) S. Sato, Y. Kwon, S. Kamisuki, N. Srivastava, Q. A. Mao, Y. Kawazoe, M. Uesugi, *J. Am. Chem. Soc.* **2007**, *129*, 873; e) M. Kuemin, S. Schweizer, C. Ochsenfeld, H. Wennemers, *J. Am. Chem. Soc.* **2009**, *131*, 15474.

[23] a) A. O. Frank, E. Otto, C. Mas-Moruno, H. B. Schiller, L. Marinelli, S. Cosconati, A. Bochen, D. Vossmeyer, G. Zahn, R. Stragies, E. Novellino, H. Kessler, *Angew. Chem. Int. Ed.* **2010**, *49*, 9278; b) F. Rechenmacher, S. Neubauer, J. Polleux, C. Mas-Moruno, M. De Simone, E. A. Cavalcanti-Adam, J. P. Spatz, R. Faessler, H. Kessler, *Angew. Chem. Int. Ed.* **2013**, *52*, 1572; c) S. Neubauer, F. Rechenmacher, A. J. Beer, F. Curnis, K. Pohle, C. D´Alessandria, H.-J. Wester, U. Reuning, A. Corti, M. Schwaiger, H. Kessler, *Angew. Chem. Int. Ed.* **2013**, DOI: 10.1002/anie.201306376.

[24] G. B. Fields, R. L. Noble, *Int. J. Pept. Protein Res.* **1990**, *35*, 161.

[25] M. Meldal, C. W. Tornoe, *Chem. Rev.* **2008**, *108*, 2952.

[26] S. Angelos, Y. W. Yang, K. Patel, J. F. Stoddart, J. I. Zink, *Angew. Chem. Int. Ed.* **2008**, *47*, 2222.

[27] a) A. El-Faham, F. Albericio, *J. Org. Chem.* **2008**, *73*, 2731; b) A. El-Faham, R. S. Funosas, R. Prohens, F. Albericio, *Chem.-Eur. J.* **2009**, *15*, 9404.

[28] R. Subiros-Funosas, R. Prohens, R. Barbas, A. El-Faham, F. Albericio, *Chem.-Eur. J.* **2009**, *15*, 9394.

[29] V. V. Rostovtsev, L. G. Green, V. V. Fokin, K. B. Sharpless, *Angew. Chem. Int. Ed.* **2002**, *41*, 2596.

[30] M. Mammen, S. K. Choi, G. M. Whitesides, *Angew. Chem. Int. Ed.* **1998**, *37*, 2755.

[31] a) H. Kessler, M. Schudok, A. Haupt, *Peptides 1988: Procedings of the 20th European Peptide Symposium, Tübingen, 1988*, (Eds: G. Jung, E. Bayer), Walter de Gruyter, Berlin, New York **1989**, 664; b) L. L. Kiessling, J. E. Gestwicki, L. E. Strong, *Curr. Opin. Chem. Biol.* **2000**, *4*, 696; c) J. E. Gestwicki, C. W. Cairo, L. E. Strong, K. A. Oetjen, L. L. Kiessling, *J. Am. Chem. Soc.* **2002**, *124*, 14922.

[32] Y. Wu, X. Z. Zhang, Z. M. Xiong, Z. Cheng, D. R. Fisher, S. Liu, S. S. Gambhir, X. Y. Chen, *J. Nucl. Med.* **2005**, *46*, 1707.

[33] C. B. Yim, I. Dijkgraaf, R. Merkx, C. Versluis, A. Eek, G. E. Mulder, D. T. S. Rijkers, O. C. Boerman, R. M. J. Liskamp, *J. Med. Chem.* **2010**, *53*, 3944.

[34] J. Blümmel, N. Perschmann, D. Aydin, J. Drinjakovic, T. Surrey, M. López-García, H. Kessler, J. P. Spatz, *Biomaterials* **2007**, *28*, 4739.

[35] a) B. T. Houseman, M. Mrksich, *Biomaterials* **2001**, *22*, 943; b) M. Kato, M. Mrksich, *Biochemistry* **2004**, *43*, 2699.

[36] E. Zamir, B. Z. Katz, S. Aota, K. M. Yamada, B. Geiger, Z. Kam, *J. Cell Sci.* **1999**, *112*, 1655.

[37] F. Chang, C. A. Lemmon, D. Park, L. H. Romer, *Mol. Biol. Cell* **2007**, *18*, 253.

[38] C. Vericat, M. E. Vela, G. Benitez, P. Carro, R. C. Salvarezza, *Chem. Soc. Rev.* **2010**, *39*, 1805.

[39] S. J. Smith, R. McCann, *Biochemistry* **2007**, *46*, 10886.

[40] R. Zaidel-Bar, C. Ballestrem, Z. Kam, B. Geiger, *J. Cell Sci.* **2003**, *116*, 4605.

[41] a) J. Spinke, M. Liley, H. J. Guder, L. Angermaier, W. Knoll, *Langmuir* **1993**, *9*, 1821; b) V. H. Pérez-Luna, M. J. O'Brien, K. A. Opperman, P. D. Hampton, G. P. López, L. A. Klumb, P. S. Stayton, *J. Am. Chem. Soc.* **1999**, *121*, 6469; c) K. Gorska, K. T. Huang, O. Chaloin, N. Winssinger, *Angew. Chem. Int. Ed.* **2009**, *48*, 7695; d) Y. Sato, K. Yoshioka, T. Murakami, S. Yoshimoto, O. Niwa, *Langmuir* **2012**, *28*, 1846.

[42] B. T. Houseman, M. Mrksich, *Angew. Chem. Int. Ed.* **1999**, *38*, 782.

[43] C. A. Widrig, C. Chung, M. D. Porter, *J. Electroanal. Chem.* **1991**, *310*, 335.

[44] M. J. Hostetler, J. E. Wingate, C. J. Zhong, J. E. Harris, R. W. Vachet, M. R. Clark, J. D. Londono, S. J. Green, J. J. Stokes, G. D. Wignall,

G. L. Glish, M. D. Porter, N. D. Evans, R. W. Murray, *Langmuir* **1998**, *14*, 17.
[45] J. Juhaniewicz, S. Sek, *Bioelectrochemistry* **2012**, *87*, 21.
[46] a) J. C. Love, L. A. Estroff, J. K. Kriebel, R. G. Nuzzo, G. M. Whitesides, *Chem. Rev.* **2005**, *105*, 1103; b) D. Samanta, A. Sarkar, *Chem. Soc. Rev.* **2011**, *40*, 2567.
[47] M. Cerruti, S. Fissolo, C. Carraro, C. Ricciardi, A. Majumdar, R. Maboudian, *Langmuir* **2008**, *24*, 10646.
[48] P. Kingshott, H. Thissen, H. J. Griesser, *Biomaterials* **2002**, *23*, 2043.
[49] a) J. Zhu, J. Zhu, T. A. Springer, *J. Cell Biol.* **2013**, *201*, 1053; b) M. A. Müller, J. Opfer, L. Brunie, L. A. Volkhardt, E. K. Sinner, D. Boettiger, A. Bochen, H. Kessler, K. E. Gottschalk, U. Reuning, *J. Mol. Biol.* **2013**, *425*, 2988.
[50] a) E. A. Evans, D. A. Calderwood, *Science* **2007**, *316*, 1148; b) I. D. Campbell, M. J. Humphries, *Cold Spring Harbor Perspectives in Biology* **2011**, *3*.
[51] a) C. Mas-Moruno, J. G. Beck, L. Doedens, A. O. Frank, L. Marinelli, S. Cosconati, E. Novellino, H. Kessler, *Angew. Chem. Int. Ed.* **2011**, *50*, 9496; b) J. Chatterjee, O. Ovadia, G. Zahn, L. Marinelli, A. Hoffman, C. Gilon, H. Kessler, *J. Med. Chem.* **2007**, *50*, 5878.
[52] Y. Liron, Y. Paran, N. G. Zatorsky, B. Geiger, Z. Kam, *J. Microsc.* **2006**, *221*, 145.
[53] M. E. Vela, H. Martin, C. Vericat, G. Andreasen, A. H. Creus, R. C. Salvarezza, *J. Phys. Chem. B* **2000**, *104*, 11878.
[54] S. Upadhyayula, T. Quinata, S. Bishop, S. Gupta, N. R. Johnson, B. Bahmani, K. Bozhilov, J. Stubbs, P. Jreij, P. Nallagatla, V. I. Vullev, *Langmuir* **2012**, *28*, 5059.